CONFINING PRESSURE EFFECTS ON MULTI-PHASE TRANSPORT IN A SHEAR-FRACTURED SANDSTONE

Sultan M. Al Enezi, Philip M. Halleck, and Abraham S. Grader
Energy Institute, Department of Energy and Mineral Engineering,
Pennsylvania State University

This paper was prepared for presentation at the International Symposium of the Society of Core Analysts held in Abu Dhabi, UAE 29 October-2 November, 2008

ABSTRACT

We have extended our earlier studies of flow in shear fractures by creating axial shear fractures and studying both single and two-phase flow behaviors, along with the effects of closure stress. A cylindrical Berea Sandstone sample was cored parallel to bedding and placed in a Hoek cell at 3.4 MPa confining stress. End loading of 23.3 kN, with oriented shims at each end, produced shear fracturing parallel to the axis and along the bedding planes. Use of a stiff testing frame allowed controlled post-failure shear displacement of 0.5 mm. The pre-fracture and post-fracture corrected gas permeabilities at 10.3 kPa were 28.9 mD and 81.5 mD, respectively, an increase in permeability of three times. A drainage and imbibition sequence using water and n-Dodecane phases, plus a controlled fractional flow experiment were conducted at 10.3 MPa confining pressure to obtain relative permeability data in the fractured rock. The absolute permeability measured by water flow was 103.4 mD. Irreducible water saturation (S_{wirr}) and residual oil saturation (S_{or}) in the fracture, obtained from X-Ray CT data, were 8.5% and 46.9%, respectively. Oil relative permeability ($k_{ro}@S_{wirr}$) was 0.93 and water relative permeability ($k_{rw}@S_{or}$) was 0.057. The former is considerably higher than typical values for non-fractured Berea, but the latter is quite similar to matrix values. This indicates that once the large fracture volumes are filled with oil, they contribute only to oil flow.

Confining pressure was then increased to 17.2 MPa to observe the effect of higher closure stress on the fracture. The sample was cleaned and the experimental sequence above repeated. The absolute (water) permeability decreased to 65.2 mD. Fractures volumes at 10.3 MPa and 17.2 MPa confining pressure were 275 mm^3 and 191 mm^3, respectively, a decrease of 30%. Aperture distribution maps at both confining pressures showed corresponding decreased average aperture width. S_{wirr} and S_{or} in the fracture were 5.9% and 40.8%, respectively. $k_{ro}@S_{wirr}$ was 0.89 and $k_{rw}@S_{or}$ was 0.064. Fluids distributions at both confining pressures confirm that most of the oil cannot be displaced out of the fracture and forces the water to flow in the matrix, thus yielding very low water relative permeabilities. Water-oil steady-state fractional flow trajectories were stable and showed a limited mobile saturation range in the fracture. The highest resistance to two-phase flow occurred at a water fractional flow of 0.95, confirming high oil occupancy in the large porosity regions of the fracture.

INTRODUCTION

Understanding multi-phase flow in fractures is important in many fields, such as ground water hydrology, contaminants clean up in soils, nuclear engineering, and in the oil industry. In petroleum reservoirs, fluid flow patterns and hydrocarbon recovery are greatly affected by fractures. Fractures can increase the permeability and enhance the recovery process however they could negatively affect the recovery process when they form bypass paths, especially in production-injection systems. Injected fluid may preferentially flow through the fractures leaving behind inaccessible hydrocarbons thus increasing the residual oil saturation. Fractures can also act as no-flow reservoir boundaries. Understanding multi-phase flow in fractured porous media will help to improve engineering simulation of multi-phase flow in fractured reservoirs.

The two basic types of fractures are tensile and shear fractures. Shear fractures occur naturally and can also occur in the near well-bore regions resulting in depletion and redistribution of insitu stress due to the well load. Transport along or across shear fractures can thus affect hydrocarbon migration and cause positive or negative skin near the well bore. Most of the work done previously has concentrated on the effects of tensile fracture on multi-phase flow. Gray et al. (1963), Barton et al. (1985), and Gentier et al. (1986) studied the effects of confining pressure on permeability of sandstones. They found that uniform loading lowers the permeability more than the non-uniform ones. Also they found that hydrostatic loading leads to maximum reduction in permeability.

To understand fluid flow behavior, Lomize (1951) and Louis (1969) developed the parallel plate model which is known as the cubic law to relate the flow rates, hydraulic head and fracture aperture. Witherspoon et al. (1980) conducted a study to validate the cubic law for fluid flow in fractured porous media. They claimed that the cubic law is valid for the samples they used although a correction factor of 1.04 to 1.65 was needed. Tsang (1984) conducted an experiment on single fracture and showed that the flow rates predicted by the cubic law were higher than the experimental flow rate. They concluded that the difference between experimental and cubic law results was due to the tortuosity which is neglected in the cubic law. Dual porosity, dual permeability mathematical modeling is widely used to simulate multi-phase flow in fractured porous media. The rock is characterized as two porous media. Different relative permeability and capillary pressure curves are used for fracture network and matrix blocks. X-shape curves are typically used for fractures. Persoff (1985) and Babadagli et al. (1992) conducted experimental studies on multi-phase flow in tensile-fractured porous media. They found that the relative permeability curve deviated from the X-shape curves typically used for fractures and found that the relative permeability curves depend strongly on flow rate, wettability, matrix saturation, permeability, and flow direction

Alvarado (2005) applied X-ray CT technology to study the mechanical and hydraulic behavior of artificial tensile fractures created in cylindrical Berea Sandstone cores under multi-phase flow. Using high resolution micro-CT allows quantification and visualization of the fracture topology and fluid distributions inside the fracture. The effects of confining pressure on

fracture morphology were studied by placing the core sample inside an x-ray transparent core holder and scanning the entire core at different confining pressures. Fractional flow experiments were conducted to study multi-phase fluid distribution between limits of the mobile saturation range. They observed order-of-magnitude variations in effective permeability under constant overall fracture saturation and flow conditions. Observations of fluid distribution in the fracture lead to the conclusion that spatial rearrangement of the non-wetting phase at constant saturation leads to these major change in effective permeability.

To characterize the aperture and visualize the fluid distributions inside the shear fracture and correlate that with the change in the permeability, a non-destructive high resolution X-ray technology has been utilized. Al Enezi (2005) conducted laboratory experiments to study the effects of a shear fracture diagonally induced in a sandstone plug cut parallel to the bedding planes. The absolute permeability as reduced by about 30% after fracturing. Also the results of multi-phase flow experiment showed that the residual fluid saturations in the matrix are significantly different than that in the fractures. The fracture was very complex because it was induced diagonally to the fluid flow axis. The inlet parts of the samples were not fractured and the outlet part had a damaged zone with multiple fractures. Due to the direction of the induced fractures, there were strong matrix/fracture interactions that made it hard to address the effects of the shear fractures on multi-phase flow.

The motivation of the present experimental work is that multi-phase flow in sheared-fractured need more investigation since most of the available papers either discussed the role of the tensile fracture or discussed the mechanical properties of shear fractures or single phase flow in shear-fractured porous media. Most of the work done concentrated on the tensile fracture that because understanding the relationship between fluid flow and geometry of shear fracture is more complicated than tensile fractures because of the need to account for the formation of gouge zones. This paper will address the rule of shear fracture in multi-phase flow in Berea Sandstone. Fluid saturations will be quantified and visualized inside the fracture. The role of confining pressure on the topology of the shear fracture and the fluid distribution inside the fracture will be addressed by conducting the two-phase flow experiments at two different pressures. To minimize the effects of matrix-fracture interaction, a shear fracture induced parallel to fluid flow path in a Berea Sandstone core sample by applying a modified shear fracturing. The results of this study have a positive contribution on the description of multi-phase fluid conductivity and distribution in rough shear fracture, which could enhance numerical modeling of fractured reservoirs and understanding the near-wellbore damage.

EXPERIMENTS

Core Preparation and Fracturing

A cylindrical Berea sandstone core (2.5 cm diameter and 7 cm long) was cut parallel to the bedding planes. The sample was surface ground and then jacketed in heat shrinkable Teflon to keep the gouge and matrix intact after fracturing. To create a shear fracture parallel to the bedding planes, the sample was shimmed using half circles of wood and metal pieces.

Then the sample was loaded in the Hoek cell and confining pressure of 500 psig (3.45 MPa) was applied. The pressurized Hoek cell was mounted inside the stiff testing machine and axial compression force was applied at a displacement rate of 0.003 mm/sec. Figure 1 shows the testing machine, and a schematic of the fracturing process. The confining pressure was maintained by a hydraulic pump. The vertical load gradually increased up to the point of failure. After failure, the sample was displaced an additional 0.50 mm to be sure that the fracture is open and connected. Figure 2 shows the development of applied axial pressure during the fracturing process.

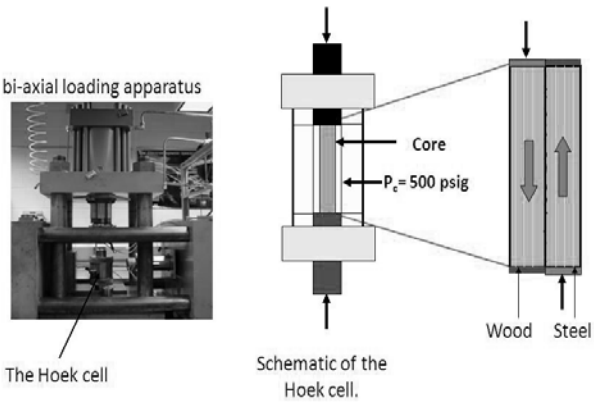

Figure 1: A: Hoek cell inside the fracturing machine, B: Schematic of the sample assembling inside the Hoek cell.

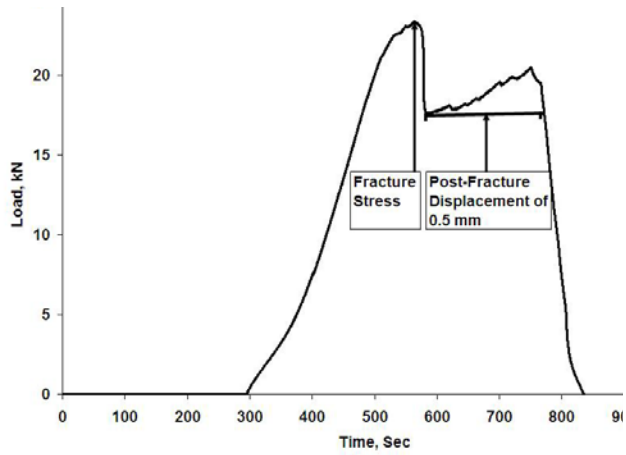

Figure 2: Stress vs. Time during fracturing.

Fluid Flow Experiment

The fractured sample was mounted inside a low x-ray attenuation carbon fiber composite core holder. The core holder was mounted inside the scanner and 1500 psig confining pressure was applied. Then four stages of fluid flow experiment were carried out. The core holder was not moved out of the scanner during the experiment to be able to compare CT images at the same scanning position and at different saturation conditions. After mounting the core holder inside the scanner and applying the confining pressure, vacuum was applied and then air permeability was measured. A dry scan of the entire sample (60 rotations and 41 slices per rotation) was acquired. Then the core plug was saturated with 5% KI brine under vacuum. Absolute permeability to brine was measured and then a full scan for the entire sample was acquired. After that oil flooding was started to bring the sample to irreducible water saturation (S_{wirr}). Several hundreds of pore volumes were injected to insure that the core is at S_{wirr} before scanning. The effective permeability of oil was measured, and then a full scan for the entire sample was acquired. A water flood was performed to bring the sample to residual oil saturation (S_{or}). Again, several hundreds of pore volumes were flooded to ensure that the core was at S_{or}. Effective permeability to water was measured and then the entire sample was scanned. In the last stage, the sample was cleaned first by injecting several hundreds of pore

volumes of alcohol, followed by injecting air for several hours and then applying vacuum for about 10 hours. Then the core was vacuum-saturated with oil. Absolute permeability to oil was measured and full scan of the sample was acquired.
After completing the fluid flow experiment at 1500 psig confining pressure, the sample was cleaned by alcohol, dried by air and vacuum, and then entire experiment sequences were repeated at a confining pressure of 2500 psig.

RESULTS AND DISCUSSIONS

Fracture Properties

The Fracture was extracted from the dry scan that consisted of 2460 images that covered the entire length of the sample. The fracture was extracted from the dry scan using commercial image processing software and by assigning a range of the CT numbers from 0 to 650 to represent the fracture. The fracture volume at 1500 psig confining pressure is 275.5 mm^3.
After increasing the confining pressure to 2500 psig, the fracture volume was reduced to 191.4 mm^3 showing 30% reduction in the fracture volume associated with the increase of the confining pressure. Figure 3 shows 2-D aperture map of the fracture at dry condition at 1500 psig (left) and at 2500 psig confining pressure (right). Figure 3 shows that the fracture is more connected and has smaller number of big asperities at 1500 psig than at 2500 psig confining pressure.

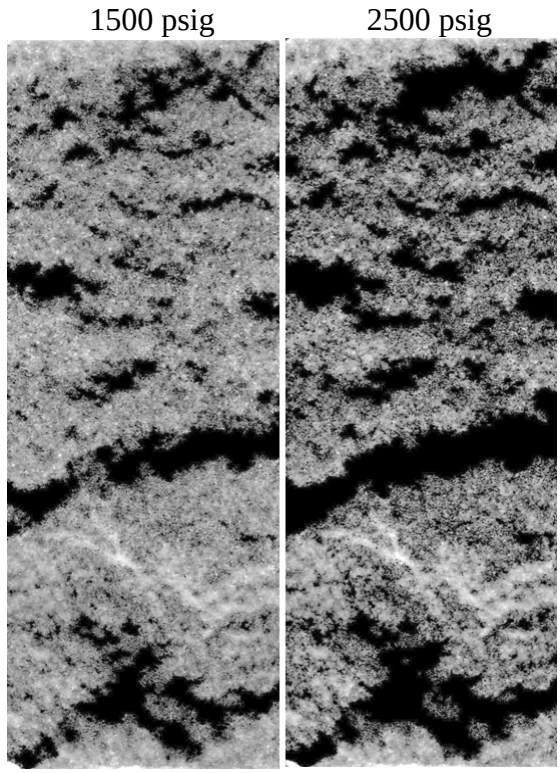

Figure 3: 2-D aperture map (The linear gray scale is between 0 and 650 microns).

Figure 4 shows computed aperture distributions at 1500 psig and 2500 psig. In the case of 1500 psig confining pressure, the average aperture width is 227 microns and the maximum fracture aperture frequency value is 0.095 for fracture aperture in the range of 8 to 10 pixels (208 to 260 microns). After increasing the confining pressure to 2500 psig, the average aperture width was reduced to 193. 2 microns, showing about 15% reduction after increasing the confining pressure and the maximum fracture aperture frequency value is 10.0 for fracture aperture in the range of 6 to 8 pixels (156 to 208 microns). It shows that there is a shift to the left after increasing the confining pressure which indicates a reduction in average aperture width.

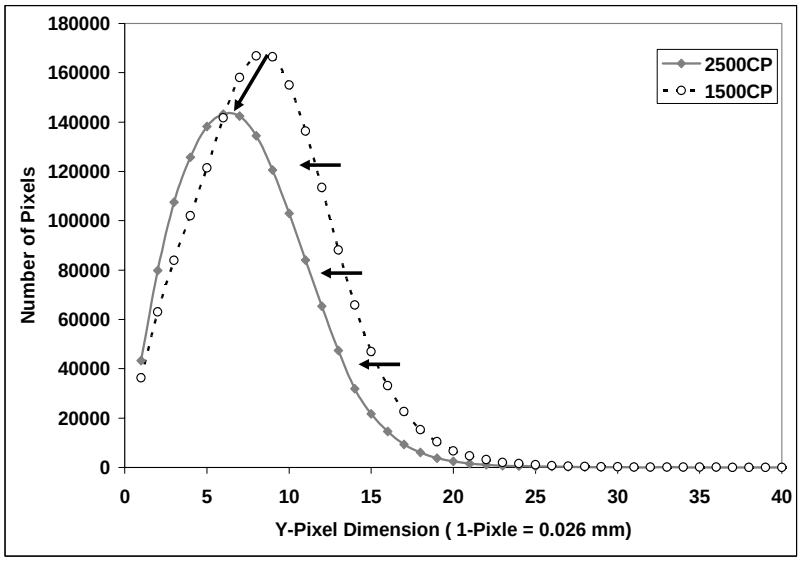

Figure 4: Aperture distribution at 1500 psig (dotted line) and 2500psig (solid line) confining pressures.

Absolute and Effective Permeabilities Measurements

The pre-fracture and post-fracture corrected gas permeabilities were measured at 1500 psig. The permeability after fracturing increases from 28.9 to 81.5 mD indicating that inducing the fracture parallel to the bedding planes increases the permeability by a factor of three. Absolute and Effective Permeabilities were measured at different saturation conditions at 1500 and 2500 psig confining pressures. The absolute permeability reduced from 103.4 mD at 1500 psig confining condition to 65.2 mD at 2500 psig, showing a 37% reduction in absolute permeability due to increasing the confining pressure. Effective permeability was measured at the end of each saturation condition at both confining pressure conditions. At 1500 psig confining pressure, oil effective permeability at S_{wirr} is 96.5 mD while the effective brine permeability at S_{or} is 5.9 mD. At 2500 psig confining pressure, oil effective permeability at S_{wirr} is 58.3 mD, showing 40 % reduction due to increasing the confining pressure. The effective water permeability at S_{or} is 4.2 mD which reduced by 29% after increasing the confining pressure. Effective permeability measurements at S_{or} condition indicate that as the large fracture volumes get saturated with oil, they contribute only to oil flow. Table 1

summarizes the results of permeability measurement during multi-phase flow experiment at 1500 and 2500 psig confining pressures.

Table 1: Absolute and effective permeability measurements at different saturation conditions at 1500 and 2500 confining pressures.

Confinig Pressure	Condition	ko, mD	kw, mD
1500 psig	100% Brine	-	103.4
	S_{wirr}	96.5	-
	S_{or}	-	5.9
	100% Oil	101.8	-
2500 psig	100% Brine	-	65.2
	S_{wirr}	58.3	-
	S_{or}	-	4.2
	100% Oil	64.1	-

Fluid Distribution at S_{wirr}

CT data were acquired at the end of each saturation condition, Dry, wet (100% brine), S_{wirr}, S_{or} and at 100% oil saturation. These data were used to map and visualize the fluid distribution at each saturation condition, especially at S_{wirr} and S_{or}. Oil and water saturations in the fracture at S_{wirr} were calculated by assigning a threshold values for each phase. After correcting the data for KI concentration, similar threshold was used at both confining pressures. Table 2 summarizes the saturation values at S_{wirr} condition. It shows that at both confining pressure, fracture has very low S_{wirr} saturation. The values of S_{wirr} were 8.50 % to 5.94 at 1500 and 2500 psig, respectively.

Table 2: Water and oil saturations at the end of oil flood at 1500 psig and 2500 psig confining pressures.

1500 psig confining	Volume,mm^3	%
Fracture	275.46	
Oil	252.05	91.50
Water	23.41	8.50
2500 psig confinig	Volume, mm^3	%
Fracture	191.42	
Oil	180.06	94.06
water	11.36	5.94

Figure 5 shows the oil and water distributions inside the fracture at S_{wirr} condition at both confining pressures. It shows that oil phase is connected and continuous through the fracture

and tends to saturate the large porosity regions in the fracture while water formed disconnected films on the wall of the fractures and tend to saturate the small apertures.

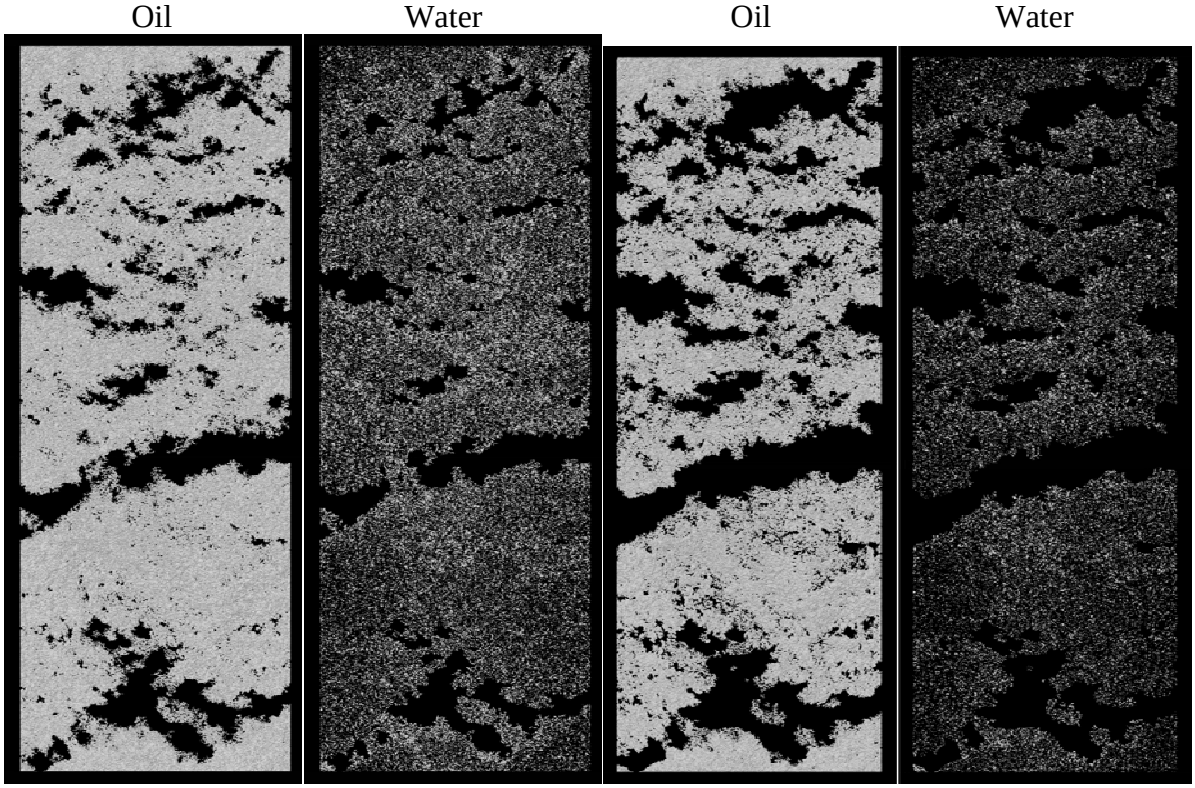

Figure 5: Fluids distributions at S_{wirr} condition at confining pressures of 1500 (left) and 2500 psig (right).

Fluid Distribution at S_{or}

Oil and water saturation were calculated using the same threshold assigned for oil and water at S_{wirr} condition**.** Table 3 summarizes the results of saturation calculation at S_{or} condition at both confining pressures. Figure 6 shows the oil and water distributions inside the fracture at S_{or} condition. Water saturation increased from 53.1 % at to 59.2 % after increasing the confining pressure from 1500 psig to 2500 psig. Visualization of fluids distributions inside the fracture showed that the oil is connected and saturated the large apertures, while the water spreads through the wall of the fracture and small cavities. Trapping the oil in the large porosity regions is responsible of lowering the water relative permeability at S_{or}. Once the oil flows into the fracture it is difficult to remove it and the water has to flow through the matrix. This explains the pressure increase during water injection and the reduction in effective brine permeability at $S_{or.}$

Table 3: Water and oil saturations at the end of oil flood at 1500 psig and 2500 psig confining pressures.

1500 psig confining	Volume,mm^3	%
Fracture	275.46	
Oil	129.15	46.89
Water	146.31	53.11
2500 psig confining	Volume, mm^3	%
Fracture	191.42	
Oil	78.10	40.80
water	113.32	59.20

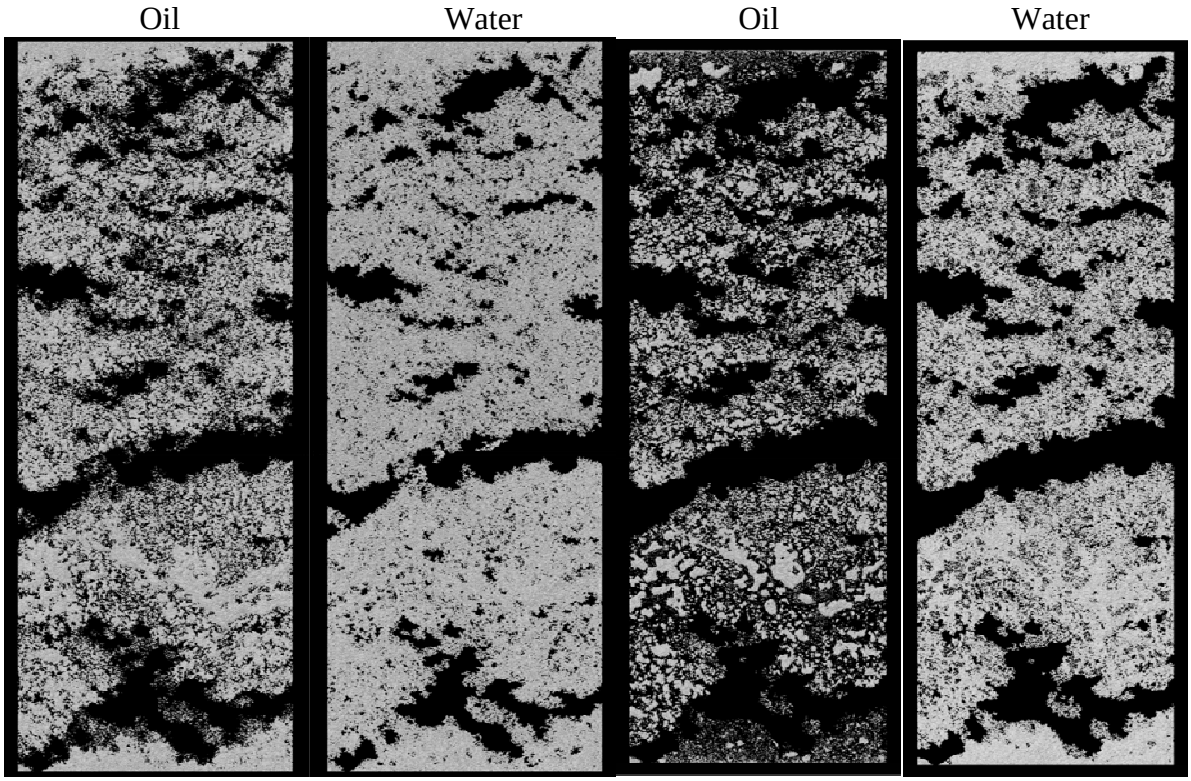

Figure 6: Fluids distributions at S_{or} condition at confining pressures of 1500 psig (left) and 2500 psig (right).

Fractional Flow Experiment

The fractional flow experiments were conducted at the end of the single-phase flow experiments. Starting with 100 % water flow, the oil flow rate was increased while decreasing the water flow rate gradually until reaching $f_w = 0.1$. Then water fractional flow was increased until reaching $f_w = 0.95$. The whole cycle was repeated several times while recording the differential pressure when it stabilized at each step. The total flow rate of 0.20 cc/min was kept constant during the experiment. Fractional flow results show that the water-oil steady-state fractional flow trajectories were stable and confirmed a limited mobile saturation range in the fracture. The highest resistance to two-phase flow occurred at a water fractional flow of 0.95, confirming high oil occupancy in the large porosity regions of the fracture.

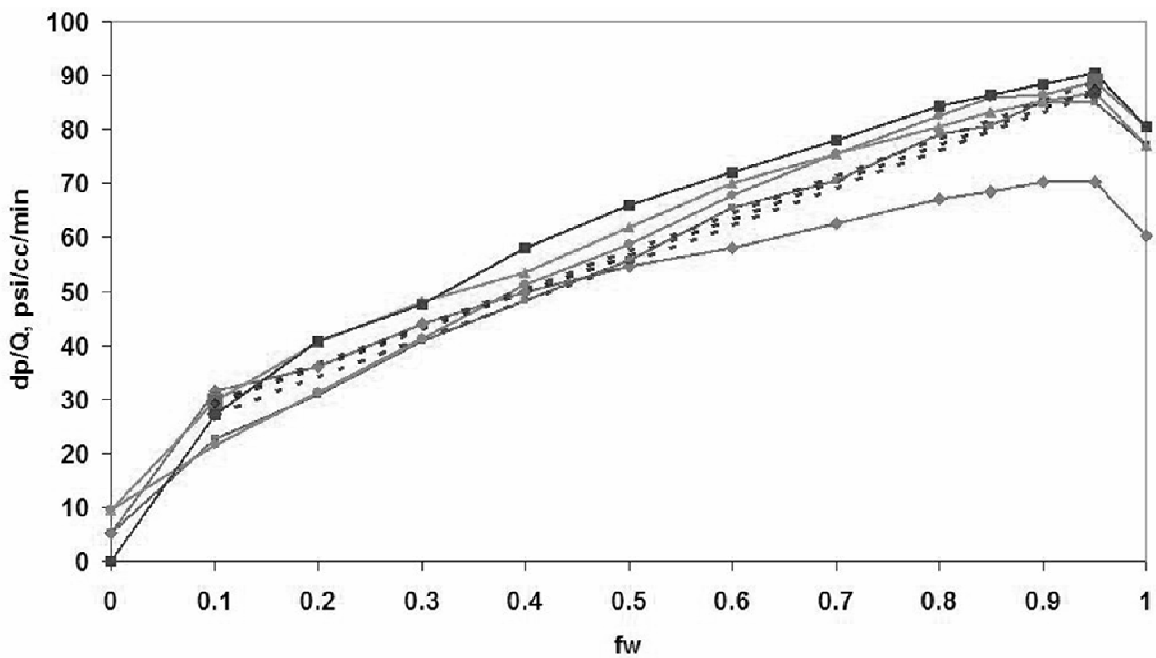

Figure 9: Normalized pressure drop vs. brine flow rate at 1500 psig confining pressure.

To address the fracture/matrix interaction, S_{wirr} and S_{or} were calculated at adjacent matrices at low and high confining pressure. The average S_{wirr} and S_{or} value were 50% and 32%, respectively. To compare water and oil saturation in the matrix adjacent to the fracture with the water and oil saturation in the non-fractured core, a two-phase flow experiment was conducted in non-fractured sample and absolute and effective permeabilities were measured at different saturation conditions during the experiment. S_{wirr} and S_{or} were 33.6% and 42.6%, respectively. S_{wirr} value is higher in the adjacent matrix because the fracture was contributing to the oil flood and the adjacent matrix had poor sweep efficiency. Water and oil relative permeabilities were 0.3 and 0.87, respectively. k_{rw} for the fractured sample and S_{or} values at

the adjacent matrix are very close to the values of the non-fractured sample because during the water flooding, the large porosity regions of the fracture were filled with oil and did not contribute to the water flood.

CONCLUSIONS

The current study documented experimental observations of 3-D fracture topology and fluid distributions inside the fracture at different saturation conditions. The results showed that as oil saturated the large porosity regions in the fracture, it is difficult to flush it out. Oil, is the non-wetting phase, tends to saturate the large aperture and the wetting phase (water) spreads along the wall of the fracture and saturate the small cavities. Relative permeability to wetting phase was drastically affected by the distribution of the non-wetting phase inside the fracture. Oil fills the middle of the fracture so that the fracture does not contributing to the water-flood. The result of this study will add valuable information to better understand the fundamental phenomena of two-fluid flow in shear fractured reservoir and though near-wellbore damage, and have positive impact of numerical modeling of such reservoirs.

REFERENCES

Al Enezi, S. M. (2005). Two Phase Flow in a Shear Fracture in a Layered Sandstone. EGEE Departement. Unviersity Park, Pennsylvania State University.

Alvarado, F. E., Grader, A. S., Halleck, P. M. "Visulization of Two-and Three-Phase Flow in Fractures Using X-Ray Computed Tomograp." (2005).

Babadagli, T. and Ershaghi, I.: "Imbibition Assisted Two-Phase Flow in Natural Fractures," SPE, 1992.

Barton, N., Bandis, S., Bakhtar, K. "Strength, Deformation and Conductivity Coupling of Rock Joints." Int. J. Rock Mech. Min. Sci. & Geomech. Abstr(1985) **22**: 121-140.

Gentier, S. a. H., D. "Mapping Fracture Aperture as a Function of Normal Stress usinga Combination of Casting, Image Analysis and Modeling Techniques." Int. J. Rock Mech. and Min. Sciences(1986) **34**: 3-4.

Gray, H. D., Fatt, I. and Bergamini. "The Effect fo Stress on Permeability of Sandstone Cores." Society of Petroleum Engineers(1963): 95-100.

Lomize, G. M.: "Flow in Fractured Rocks" (in Russian). Gosenergoizdat, Moscow**:** 127, 1951.

Louis, C.: "A study of groundwater flow in jointed rock and its influence on the stability of rock masses," Rock Mech. Res **Rep. 10**: 90, 1969.

Persoff, P. and Pruess, K.: "Two-Phase Flow Visualization and Relative Permeability Measurements in Natural Rough-Walled Rock Fractures," Water Resources Research **31 (5)**, 1985.

Tsang, Y. W.: "The effect of tortuosity on fluid flow through a single fracture," Water Resources Research **20 (9)**: 1209-1215, 1984.
Witherspoon, P. A., Wang, J. S. Y., Iwai, K. and Gale, J. E.: "Validity of cubic law for fluid flow in a deformable rock fracture," Water Resources Research **16**: 1016-1024, 1980.